

Low-Rank Adaptation of Neural Fields

ANH TRUONG, Massachusetts Institute of Technology, USA
 AHMED H. MAHMOUD, Massachusetts Institute of Technology, USA
 MINA KONAKOVIĆ LUKOVIĆ, Massachusetts Institute of Technology, USA
 JUSTIN SOLOMON, Massachusetts Institute of Technology, USA

Processing visual data often involves small adjustments or sequences of changes, such as in image filtering, surface smoothing, and video storage. While established graphics techniques like normal mapping and video compression exploit redundancy to encode such small changes efficiently, the problem of encoding small changes to neural fields (NF)—neural network parameterizations of visual or physical functions—has received less attention. We propose a parameter-efficient strategy for updating neural fields using low-rank adaptations (LoRA). LoRA, a method from the parameter-efficient fine-tuning LLM community, encodes small updates to pre-trained models with minimal computational overhead. We adapt LoRA to instance-specific neural fields, avoiding the need for large pre-trained models yielding a pipeline suitable for low-compute hardware. We validate our approach with experiments in image filtering, video compression, and geometry editing, demonstrating its effectiveness and versatility for representing neural field updates.

CCS Concepts: • **Computing methodologies** → **Neural networks**.

Additional Key Words and Phrases: neural fields, low-rank adaptation, geometry, graphics, compression

ACM Reference Format:

Anh Truong, Ahmed H. Mahmoud, Mina Konaković Luković, and Justin Solomon. 2025. Low-Rank Adaptation of Neural Fields. *ACM Trans. Graph.* 1, 1 (April 2025), 10 pages. <https://doi.org/10.1145/nnnnnnn.nnnnnnn>

1 INTRODUCTION

Processing visual data often involves small adjustments or sequences of changes, such as in image filtering, surface smoothing, and video storage. For example, image filtering usually involves local operations that alter the appearance but preserve the overall structure of an input image. Similarly, local surface edits—such as smoothing or sharpening—yield perturbative displacements from the original surface. Finally, videos consist of image frames where the difference between any two consecutive frames is likely small.

Small changes should be able to be stored compactly. Built on this observation, classical methods in graphics reduce redundancy for different representations by only storing what is necessary to realize a change. For instance, normal maps store surface displacements as compact textures encoding bumps and dents. Similarly, video

Authors' addresses: Anh Truong, Department of Electrical Engineering and Computer Science, Massachusetts Institute of Technology, 32 Vassar St, Cambridge, MA, 02139, USA, anh_t@mit.edu; Ahmed H. Mahmoud, Computer Science & Artificial Intelligence Laboratory, Massachusetts Institute of Technology, 32 Vassar St, Cambridge, MA, 02139, USA, ahdhn@mit.edu; Mina Konaković Luković, Department of Electrical Engineering and Computer Science, Massachusetts Institute of Technology, 32 Vassar St, Cambridge, MA, 02139, USA, minakl@mit.edu; Justin Solomon, Department of Electrical Engineering and Computer Science, Massachusetts Institute of Technology, 32 Vassar St, Cambridge, MA, 02139, USA, jsolomon@mit.edu.

© 2025 Association for Computing Machinery.

This is the author's version of the work. It is posted here for your personal use. Not for redistribution. The definitive Version of Record was published in *ACM Transactions on Graphics*, <https://doi.org/10.1145/nnnnnnn.nnnnnnn>.

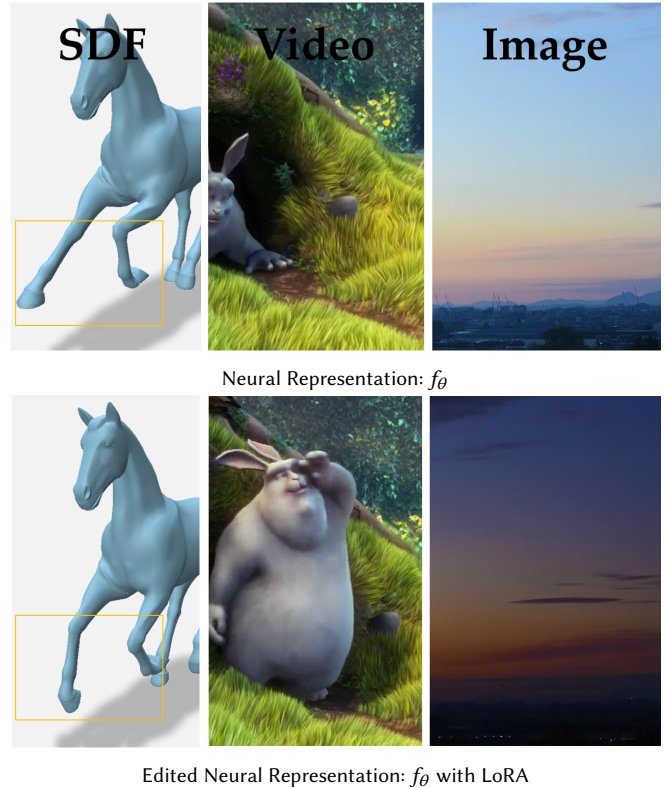


Fig. 1. Overview of our method. We encode edits to an instance-specific neural field (e.g., SDF, image color) as parameter-efficient low-rank adapters. Compared to standard fine-tuning, our method optimizes $\approx 8\times$ fewer parameters while achieving comparable fidelity.

codecs reduce temporal redundancy by using intermediate P-frames that store offsets from previous frames. In contrast, methods for compactly perturbing neural fields—an emerging representation in graphics and vision—have received little attention.

Neural fields represent physical or visual quantities (e.g., signed distances, density, color) in the weights of neural networks [Takikawa et al. 2023]. Neural fields have desirable properties (e.g., continuity, differentiability, compact size, and ease of querying) that make them attractive for visual computing applications like deformation [Mehta et al. 2022], elastic simulation [Modi et al. 2024], and image processing [Luzi et al. 2024]. Like the classical examples above, many of these tasks yield small updates to a pre-trained model.

Editing a neural field, however, is far from straightforward, as there is a highly non-linear relationship between changes in its weights and the resulting changes in the output. Many specialized

methods have been proposed to edit specific classes of neural fields (e.g., NeRFs [Liu et al. 2021] and neural SDFs [Wang et al. 2021]) but require large memory footprints and/or elaborate training pipelines (e.g., involving full fine-tuning or auxiliary networks).

As a generic alternative, we present a parameter-efficient strategy for updating neural fields to capture small changes in the input function using low-rank adaptations (LoRA) [Hu et al. 2022]. LoRA is a hugely popular method for parameter-efficient fine-tuning of Large Language Models (LLMs), which aims to fine-tune a pre-trained network on a similar data distribution using relatively few parameters. Our key insight is that typical updates to the function represented by a neural field (e.g., a filtered image) correspond to small updates in the sampled data distribution; hence, strategies from parameter-efficient fine-tuning like LoRA are relevant.

Unlike existing LoRA-based methods for visual data (e.g., image stylization LoRAs [Liu et al. 2024a; Shah et al. 2025]), which operate in the weight space of a **large** pre-trained model trained on a collection of instances (e.g., many entire images), we operate in the weight space of an instance-specific neural field (e.g., a neural field overfit to an image that maps pixel coordinates to their corresponding colors). This new setting is valuable because large pre-trained models are unnecessary for common types of edits in graphics and can be prohibitive on low-compute hardware.

We demonstrate the effectiveness and versatility of LoRAs for neural field updates with experiments in image, geometry, and video applications. Our experiments indicate that our method can effectively adapt pre-trained neural fields to faithfully encode edits while using 7-8× **fewer parameters than conventional fine-tuning**.

In summary, our contributions are:

- A parameter-efficient strategy for perturbing a neural field using low-rank adaptations (LoRA)
- Experimental results validating the effectiveness and versatility of LoRAs for neural field updates in image filtering, video compression, and geometry editing (Figure 1).

2 RELATED WORKS

2.1 Neural Fields

Neural fields are coordinate-based neural networks that have received significant attention as a flexible representation for data in visual computing [Takikawa et al. 2023]. By representing spatially- and time-varying physical properties of scenes or objects that may not have known analytic forms, neural fields are useful in many applications such as surface modeling [Park et al. 2019], scene reconstruction [Mescheder et al. 2019], inverse rendering [Mildenhall et al. 2021], signal processing [Sitzmann et al. 2020], and physics-informed problems [Raissi et al. 2019]. Neural fields have several desirable properties: they are continuous, fully differentiable, and can do not rely on costly spatial discretizations.

Neural fields typically approximate either a single instance of data (e.g., a single image or surface) by directly “overfitting,” or a collection of instances using a shared network with instance-specific latent codes [Park et al. 2019]. While initially dismissed as impractical, instance-specific neural fields have proven effective as a primary representation of graphics data [Davies et al. 2020]: these networks are not required to generalize across instances, allowing

a single instance to be independently parametrized by the full network. Once trained, these networks can act as a drop-in replacement for the signal they encode; for example, a neural signed distance function (SDF) is immediately usable for downstream tasks in geometry processing such as performing fast closest-point queries or CSG operations. These instance-specific neural fields tend to be memory-efficient compared to standard representations in graphics. Several works explore lossy data compression via compression of neural field weights using techniques such as weight quantization, model pruning [Chen et al. 2021], and low-rank tensor factorizations [Chen et al. 2022]. We focus on instance-specific neural fields.

Leveraging the universal approximation theorem [Kim and Adali 2003], many works parametrize fields using multi-layer perceptrons (MLP). Although augmenting MLP networks with auxiliary data structures—such as grids of latent vectors [Martel et al. 2021; Müller et al. 2022; Sivgin et al. 2024] or sparse hierarchies [Takikawa et al. 2021]—has become standard practice for accelerating training, these require a substantial memory footprint, limiting their use in low-compute hardware. We therefore restrict the scope of our method to MLP-based neural fields.

2.2 Neural Field Editing

Editing a neural field to fit new observed data is not straightforward, as there is a highly non-linear relationship between changes in its weights and the resulting changes in the network output. Recent works have proposed neural field editing techniques that fall under three broad categories [Takikawa et al. 2023]: (1) network fine-tuning, where parameters of a pre-trained neural field are further optimized to fit edited data observations [Liu et al. 2021]; (2) using hypernetworks trained to map data distributions to neural field parameters [Chiang et al. 2022]; (3) latent code fine-tuning/interpolation for networks conditioned on latent codes [Hao et al. 2020]. Our investigation focuses on network fine-tuning, because hypernetworks require access to a data distribution which may be unavailable and unwanted for performing simple edits, and latent-code models are outside the scope of this work (see §2.1).

Closest to our approach, prior works in neural field fine-tuning have explored applying updates to a subset of a pre-trained neural field’s parameters. Liu et al. [2021] propose fine-tuning later layers of a pre-trained NeRF jointly with their latent codes. Their hybrid approach allows them to avoid the cost of fully fine-tuning the network, but earlier layers remain fixed by construction and therefore limit the expressivity of the network update. [Mazzucchelli et al. 2024] observe that neurons in the final layer of a NeRF’s color MLP encode either view-dependent or diffuse appearance. By selectively fine-tuning only the neurons associated with diffuse appearance, their method is able to quickly re-color scenes encoded by a NeRF. Both of these methods, however, assume that the pre-trained model has a typical NeRF architecture. We are not aware of generic parameter-efficient methods for updating neural fields.

2.3 Low-Rank Adaptations

Low-rank adaptation (LoRA) [Hu et al. 2022] is a widely-used strategy for parameter-efficient fine-tuning of foundation models like large language models (LLMs). By imposing a low-rank constraint

on model weight updates, LoRA has proven effective in adapting pre-trained models to downstream tasks while requiring few additional parameters. Beyond their original setting in LLM fine-tuning, LoRAs have been applied to other foundation models, predominantly diffusion models for image and 3D data [Dagli et al. 2024; Lu et al. 2024] in tasks such as stylization [Liu et al. 2024b], text-based editing [Qi et al. 2024], and generative modeling [Wang et al. 2024].

While prior art demonstrate impressive task adaptation using LoRA, they assume access to a **large-scale** pre-trained model, often with billions of parameters. Access to such models requires significant computational resources and—more importantly—is unwieldy for encoding direct edits to small networks such as neural fields. In this work, we investigate the use of LoRA for parameter-efficient editing of instance-specific neural fields.

In the following, we first review neural fields (§3), describe our LoRA-based strategy for updating generic neural fields (§4) and its implementation for specific types of fields (§5), and lastly discuss our experimental findings (§6).

3 PRELIMINARIES

In this section, we establish notation used in the rest of the paper. Let $f_\theta : \mathbb{R}^m \rightarrow \mathbb{R}^n$ denote a neural field, i.e., a continuous function of space parameterized by the weights θ of a neural network, where m and n are defined by the target field. For example, a signed distance function (SDF) of a closed surface in space has $m = 3$ and $n = 1$, as it maps a 3D spatial coordinate to its corresponding signed distance to the surface. An RGB image has $m = 2$ and $n = 3$, as it can be viewed as a map from 2D coordinates to RGB triplets. We assume that f_θ is overfit to a *single* instance of graphics data, e.g., a single image. This overfitting typically involves minimizing the reconstruction error of the neural field with respect to the target field over θ .

While numerous architectures exist for different types of field data, we consider the most fundamental: a multi-layer perceptron (MLP) that maps spatial coordinates to field values. MLPs simply alternate between linear layers and elementwise non-linearities, e.g., the ReLU activation function. Similar to previous work [Mildenhall et al. 2021; Müller et al. 2022], before evaluating the MLP, we apply a frequency/positional encoding γ to lift the input coordinates to a higher-dimensional space:

$$\gamma(x) := (\sin(2^0 x), \cos(2^0 x), \sin(2^1 x), \cos(2^1 x), \dots, \sin(2^{L-1} x), \cos(2^{L-1} x)),$$

where $L \in \mathbb{N}$. Frequency encodings have proven effective in helping MLPs to regress high-frequency content. Composing the steps of our construction, we therefore consider neural fields of the form $f_\theta(x) := \text{MLP}_\theta(\gamma(x))$.

4 LOW-RANK ADAPTATION OF NEURAL FIELDS

The input to our method consists of (1) a neural field f_θ representing a single graphics instance \mathcal{D} (e.g., an image or an SDF) and (2) an edited variant \mathcal{D}' of \mathcal{D} . The type of edit depends on the application; and we provide several examples in §5. Our method outputs a set of additive weight updates to f_θ as low-rank adapters, defined below. When these updates are applied to f_θ , they approximate the edited

instance \mathcal{D}' . This approach encodes the *small* edit made to \mathcal{D} as a low-rank update to the base neural field f_θ (see Figure 1).

As discussed in §2, existing methods primarily update neural fields by fine-tuning the network on newly-observed data. This approach typically involves either storing a full copy of the base model weights or discarding the original model entirely. Neither of these options is ideal: storing a complete copy is often redundant, especially for minor edits, while losing access to the base model eliminates the ability to encode multiple edits from a shared starting point. Drawing inspiration from recent advances in parameter-efficient fine-tuning, we address this challenge by leveraging **low-rank adaptations** applied to neural fields.

A low-rank adapter (LoRA) for a pre-trained neural network is a rank-constrained additive update to its weight matrices. To define this update, recall that an MLP with $h + 1$ layers can be written in the following form:

$$\text{MLP}_\theta(x) = W_h \sigma(W_{h-1} \sigma(W_{h-2} \sigma(\dots (W_1 \sigma(W_0 x)) \dots))), \quad (1)$$

where the matrices W_i contain weights of the neural network and $\sigma(\cdot)$ is an activation; θ contains the elements of the matrices W_i .

Let $W_i \in \mathbb{R}^{d_i^{\text{out}} \times d_i^{\text{in}}}$ be one of the weight matrices in $\{W_0, \dots, W_h\}$ of a pre-trained network; W_i performs a linear transformation from $\mathbb{R}^{d_i^{\text{in}}}$ to $\mathbb{R}^{d_i^{\text{out}}}$. Rather than fine-tuning the W_i matrices directly, we fine-tune the network by updating $W_i \mapsto W_i + \Delta W_i$, where W_i remains fixed and its adapter ΔW_i satisfies

$$\text{rank}(\Delta W_i) < \min\{d_i^{\text{in}}, d_i^{\text{out}}\}.$$

In particular, drawing inspiration from Hu et al. [2022], we factorize

$$\Delta W_i := B_i A_i, \quad (2)$$

where $A_i \in \mathbb{R}^{r \times d_i^{\text{in}}}$, $B_i \in \mathbb{R}^{d_i^{\text{out}} \times r}$, and r is an adjustable parameter. By construction, the rank of the weight update ΔW is at most r .

While prior methods predominantly apply LoRA to large foundation models trained on extensive datasets, we *apply LoRA directly to the weights of a neural field to encode edits to the field compactly*. That is, given a pre-trained neural field f_θ representing a graphics instance \mathcal{D} as well as an edited version \mathcal{D}' , we encode the change from \mathcal{D} to \mathcal{D}' as a LoRA applied to f_θ . By analogy, the LoRA is to f_θ as the edit is to \mathcal{D} .

By encoding edits to a neural field as LoRAs, we inherit many of the advantages LoRAs offer in their original context of LLMs. Since LoRAs generalize full fine-tuning (by setting $r = \min\{d_i^{\text{in}}, d_i^{\text{out}}\}$), they enable finer control over the tradeoff between memory footprint and the expressiveness of the network update. For a pre-trained weight matrix $W_0 \in \mathbb{R}^{d_i^{\text{out}} \times d_i^{\text{in}}}$, a rank- r LoRA requires only $r(d_i^{\text{in}} + d_i^{\text{out}})$ parameters, which is significantly fewer than the $d_i^{\text{out}} \times d_i^{\text{in}}$ parameters needed for full fine-tuning, especially when $r \ll d_i^{\text{in}} d_i^{\text{out}} / (d_i^{\text{in}} + d_i^{\text{out}})$.

In our approach, we focus on simple edits, where the information contained in the pre-trained neural field remains relevant. Under this assumption, LoRAs are a natural fit, as they are designed to capture incremental changes to the pre-trained network. Furthermore, as edits are translated into weight updates for a neural field, downstream tasks can be performed by directly querying the LoRA-updated neural field without reference to the original data \mathcal{D} , \mathcal{D}' .

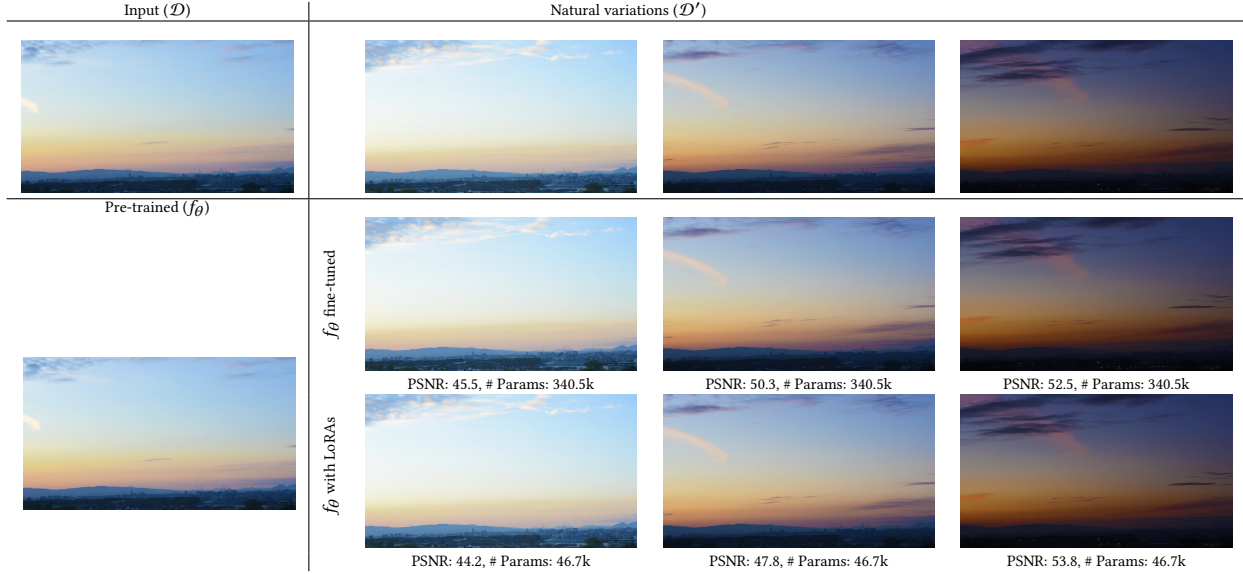


Fig. 2. We encode natural variations \mathcal{D}' of a base image \mathcal{D} (top row) by fully fine-tuning a pre-trained neural field f_θ overfit to \mathcal{D} (middle row), or by optimizing low-rank adapters to f_θ (bottom row). Using only 15% of the number of parameters required for full-finetuning, our LoRA updates are able to reconstruct the variations with comparable accuracy (PSNR). Photos taken by Geri Toth.

5 ENCODING VISUAL DATA VARIATIONS WITH LORA

In this section, we explore three graphics representations where our LoRA-based representation can capture changes.

5.1 Geometric Deformations

Geometry processing applications are rife with settings where shapes undergo relatively minor edits or changes that each need to be represented and stored. For example, subsequent frames of an animated sequence of surfaces differ by relatively small displacements. Similarly, geometry filters like smoothing [Desbrun et al. 1999], stylization [Liu and Jacobson 2019, 2021], developable approximation [Sellán et al. 2020; Stein et al. 2018], and conformal flows [Crane et al. 2013; Kazhdan et al. 2012] generate relatively small offsets of surfaces in the process of iteratively optimizing a given functional.

Linking these applications to the setting of neural fields, we encode input surfaces \mathcal{D} as neural networks f_θ that contain \mathcal{D} as a level set of a signed distance function (SDF) [Park et al. 2019] or occupancy field [Mescheder et al. 2019]. We generate edits to \mathcal{D} as surface deformations using standard modeling tools such as cage-based or as-rigid-as-possible deformation [Igarashi et al. 2005; Sorkine and Alexa 2007]; since our goal is to examine the capacity of our representation rather than to design a surface editing pipeline, we perform these deformations on a meshed version of \mathcal{D} .

To encode the deformation of \mathcal{D} as an update to f_θ , we optimize for LoRA parameters A_i, B_i by minimizing \mathcal{L} used to obtain f_θ , but with field values sampled using the deformed surface \mathcal{D}' :

$$\min_{\{A_i\}_{i=0}^h, \{B_i\}_{i=0}^h} \sum_{x \in \mathcal{X}} \mathcal{L}(f_{\theta+\text{LoRA}}(x), \mathcal{D}'_x) \quad (3)$$

where \mathcal{X} is a dense set of 3D point samples, \mathcal{D}'_x denotes the target field value at a $x \in \mathcal{X}$ evaluated using \mathcal{D}' (e.g., signed distance

to \mathcal{D}' from x), and $f_{\theta+\text{LoRA}}$ denotes f_θ with the pre-trained parameters $\theta = (W_0, \dots, W_h)$ frozen and a trainable LoRA update $((A_0, B_0), \dots, (A_h, B_h))$ applied to every weight matrix. We rescale geometry to fit in the box $[-1, 1]^3$.

We compute SDF values using PySDF. As suggested by Müller et al. [2022], our reconstruction loss \mathcal{L} is the mean average percentage error (MAPE), defined as $\frac{|\text{prediction} - \text{target}|}{|\text{target}| + 0.01}$, both for optimizing the initial model parameters θ and the LoRA updates (A_i, B_i) .

5.2 Image Variations

Imaging applications also yield sequences or collections of small changes to an initial image, inspiring applications of LoRA when the images are encoded as neural fields. Given the popularity of neural networks in computer vision, there are countless applications that could benefit from our constructions. As discussed in §2.1, we focus on the setting where a network is “overfit” to a single image, used in applications like compression [Davies et al. 2020] and superresolution [Ulyanov et al. 2018].

Mechanically, our experiments in image processing are implemented using a similar approach to the experiments using neural fields in §5.1. In this case, \mathcal{D} samples pixel values in two-dimensional space instead of SDFs or occupancies in a volume. During training, we extend images from the discrete pixel grid to real-valued coordinates using bilinear interpolation.

We represent changes to an input image $\mathcal{D} \in \mathbb{R}^{H \times W}$ as updates to an MLP f_θ , which in this case maps from (sub-)pixel locations to RGB values. The changes can be post-process edits done in image processing software (e.g., filtering) or may also arise from natural variations in image content (e.g., different lighting conditions in camera-captured images). We optimize for LoRA parameters using

the formulation in equation (3), where our reconstruction loss \mathcal{L} is the relative L2 loss, and \mathcal{X} is replaced by a set of 2D point samples in $[H, W]^2$ drawn uniformly at random and rescaled to $[-1, 1]^2$; \mathcal{D}'_x is the (interpolated) RGB value of the varied image \mathcal{D}' at $x \in \mathcal{X}$.

5.3 Video

Probably the most self-evident application of our methodology in visual computing is to video data. In between cuts and changes in camera angles, subsequent frames in a video sequence are typically small perturbations of each other, in either the spatial displacement sense (moving characters) or in pixel color (changing lighting conditions). Indeed, MPEG and other video compression codecs leverage this structure by encoding the differences and/or displacements between adjacent frames in short sequences rather than the grid of absolute pixel colors. In our case, LoRA updates hold promise of capturing small spatial and color variations between frames, since the early layers of the network are transforming the input coordinates x and the later layers eventually produce an RGB value $f_\theta(x)$.

To derive our training procedure, we view videos as a special case of image variations (§5.2), where frame-to-frame differences are induced by time-varying content. Given f_θ representing a video frame $\mathcal{D} \in \mathbb{R}^{H \times W}$, we take \mathcal{D}' to be a subsequent frame from the same sequence. We encode the frame-to-frame variation by again optimizing for LoRA parameters using equation (3).

As a stress test for our approach and to demonstrate a possible application, we propose to encode sequential video frames by *composing* LoRAs. Inspired by traditional video codecs, which interleave (1) complete images (I-frames) and (2) predicted images (P-frames) storing only changes from their previous frame, we analogously represent a video as (1) f_θ for an initial (I-)frame, and (2) a sequence of LoRAs, one for each subsequent (P-)frame. In total, this means that frame k in a sequence is a rank- $r(k-1)$ update of frame 1 in the sequence, since each LoRA update induces a change of rank- r .

In more detail, suppose the target video contains n frames. As an initial step, we overfit $f_{\theta,1}$ to frame 1, optimizing the parameters in θ . Next, a LoRA is optimized to encode the update to f_θ to reconstruct frame 2. This LoRA can be summed with θ to yield a new “pre-trained” model $f_{\theta,2}$. After freezing these parameters for $f_{\theta,2}$, we optimize a subsequent LoRA to reach frame 3. This procedure continues until every frame $i \in \{2, \dots, n\}$ is associated with a LoRA-encoded offset from its previous frame.

REMARK. *Our proposed pipeline for representing subsequent frames optimizes them one-at-a-time. This algorithm has identical efficiency per frame as the static experiments in the previous two subsections. An alternative strategy might jointly train θ and the sequence of LoRAs over the entire sequence in one shot; while in principle this approach could achieve lower error and avoid error accumulation as a sequence progresses, it is far more expensive (updates to frame n have to back-propagate back to frame 0). Our experiments in §6.2 demonstrate that our simpler approach is sufficient.*

6 EXPERIMENTS

To demonstrate the versatility of LoRA for encoding variations in neural fields, we perform experiments with three common types of graphics data as described in §5: surfaces, images, and videos.

6.1 Experimental Setup

Baselines. Across all types of data, we compare the performance of encoding variations using LoRA against fine-tuning the full base neural field f_θ , the current standard approach for directly editing generic neural fields. Additionally, to determine whether the low-rank constraint on the weight updates ΔW encourages ΔW to encode a minor *offset* from \mathcal{D} rather than representing the *entire* edited instance \mathcal{D}' , we perform a fixed-parameter-count comparison: we compare the reconstruction quality of \mathcal{D}' using a LoRA-augmented base model $f_{\theta, \text{LoRA}}$ against that using a new neural field $f_{\theta'}$ trained from scratch with the same number of parameters as the LoRA (i.e. $\text{size}(\text{LoRA}) = \text{size}(\theta')$). $f_{\theta'}$ has the same architecture as f_θ but a uniformly lower hidden dimension size, which selected so that $f_{\theta'}$ has a parameter count as close to $\text{size}(\text{LoRA})$ as possible.

Metrics. For surface fitting, we measure the fidelity of the zero level set of our LoRA-augmented neural SDFs to the reference edited surface \mathcal{D}' using the intersection-over-union (IoU) metric. Following Müller et al. [2022], we compute IoU by comparing the signs of SDFs at 134 million points uniformly distributed in the bounding box of the mesh. IoU ranges from 0 to 1, with 1 indicating a perfect fit. For images, we report the peak-signal-to-noise (PSNR) between the reconstructed and reference images. Lastly, we measure the mean PSNR across all frames in our video experiments.

Architecture. In all experiments, we use a standard MLP for our base models f_θ with a frequency encoding (§3) and ReLU activations on the hidden layers. We use 4, 5, and 6 hidden layers for SDF, image, and video data, resp., all with a hidden layer width of 256. For the frequency encoding, we use $L = 6$ for SDF experiments and $L = 10$ elsewhere. For our low-rank adapters, we use a default rank $r = 16$. This rank provides $8\times$ reduction in the number of parameters for a pre-trained hidden layer weight $W_i \in \mathbb{R}^{256 \times 256}$ compared to full fine-tuning. We found these to be effective default settings with minimal hyperparameter tuning. In practice, one could select base model hyperparameters according to the complexity of the input data and set r based on the magnitude of the edit.

Initialization. Following Hayou et al. [2024], we initialize each A_i matrix of our LoRAs using a normal distribution $\mathcal{N}(0, 1/d_i^{in})$ where d_i^{in} is the input dimension of the corresponding base weight $W_i \in \mathbb{R}^{d_i^{out} \times d_i^{in}}$; every B matrix is initialized to 0. The update $\Delta W_i = B_i A_i$ is scaled by $1/r_i$ where r_i is the rank of the current adapter.

Implementation details. We implement our base neural field and LoRA updates in PyTorch. Experiments are carried out on a machine with a NVIDIA RTX3090 GPU, with 24GB of memory and 1395MHz clock speed. We compute SDF samples from meshes using the PySDF Python library. We train using the Adam algorithm [Kingma 2014]. We observed reasonably fast convergence with a learning rate of 10^{-4} for training the base neural field f_θ and 5^{-2} for LoRA parameters. For fairness, we use the same learning rate for both our LoRA and full fine-tuning experiments.

6.2 Results

Geometric deformations. We perform ARAP deformation on an armadillo mesh with its legs fixed and use cage-based deformation

	Frame #1	Frame #25	Frame #50	Frame #99
Ground Truth				
f_{θ} fine-tuned				
	PSNR: 41.5 dB, # Params: 406.1k	PSNR: 42.6 dB, # Params: 406.1k	PSNR: 43.4 dB, # Params: 406.1k	PSNR: 43.9 dB, # Params: 406.1k
f_{θ} with LoRAs				
	PSNR: 39.1 dB, # Params: 54.6k	PSNR: 39.0 dB, # Params: 54.6k	PSNR: 39.2 dB, # Params: 54.6k	PSNR: 39.2 dB, # Params: 54.6k

Fig. 3. We encode a high-resolution video as accumulative LoRA updates from an initial frame (see §5.3). Here we visualize reconstructions of four frames using full fine-tuning per frame vs. our LoRA-based encoding method and report the reconstruction accuracy alongside parameter counts.

on horse and penguin meshes. Figure 4 shows that the IoU for LoRA and full fine-tuning reconstructions differ by 0.02 after training; each approach has the same training step budget. Qualitatively, both methods faithfully encode the edited surfaces, preserving high-frequency details like the ridges on the armadillo. Our LoRA updates, however, use *with 85-90% fewer parameters* than full fine-tuning. Minor noisy artifacts are visible on the armadillo for *both* approaches: these are present globally on the fully fine-tuned surface but are concentrated in the upper half on the LoRA-reconstructed surface, coinciding with the region of largest deformation.

Our LoRA updates not only yield comparable reconstruction quality at the end of training but also exhibit faster and stabler convergence than full fine-tuning (Figure 6): LoRA reconstruction error drops sharply near the beginning of optimization followed by gradual but consistent improvement, whereas fine-tuning takes more steps to reach a comparable loss while experiencing more variance. Qualitatively, Figure 6 also shows that our LoRA updates begin to identifiably approximate the deformed surface in as few as 100 iterations, while fine-tuning struggles. Fine-tuning causes the encoded surface to deviate drastically from the base surface near the beginning of optimization, before resolving to the deformed surface. On the other hand, in-training artifacts from LoRA are localized to spatial regions where the deformation is largest, and unmodified regions remain almost fully intact.

Image variations. For the task of encoding natural variations of an image, we use four camera-captured 1920×1080 photos of a sunset at different points in time with a fixed viewpoint. We pick one of the intermediate photos as our base image. As in Figure 5, our LoRAs achieve PSNR values comparable to full fine-tuning—in some cases slightly exceeding it—with $8\times$ fewer parameters. Visually,

the LoRA reconstructions indistinguishable from the fine-tuning reconstructions; our LoRAs faithfully represent changes in lighting conditions and image content (e.g., moving clouds). Next, for the task of encoding digitally-stylized variations of a base image, we apply oil-painting and watercolor filters from commercial software to generate variations. Figure 10 shows that there is a more noticeable PSNR gap with our LoRAs; our reconstructions capture the style but to a smaller degree compared to fine-tuning.

We conduct the fixed parameter-count baseline described in §6.1 on a difficult input image where the base model is barely able to fit to the input. Figure 9 shows a decrease in reconstruction quality for both our LoRAs and the small MLP baseline, as expected. However, with the same number of parameters, our LoRAs visibly preserve details that the baseline cannot resolve, outperforming the baseline by 1.9 dB.

Video fitting. We apply the sequential LoRA optimization procedure outlined in §5.3 to encode real video footage (Figure 3) as well as an animated sequence (Figure 8) containing 100 and 130 frames, respectively. Even with basic sequential optimization of LoRAs, our method is able to encode long sequences of frame-to-frame changes with no apparent long-term error accumulation (Figure 7); while there is local fluctuation between small subsequences of frames, we see that the frame reconstruction accuracy remains within 39.2 ± 1 dB across all 100 frames using our default configuration ($r = 16$) for captured footage, and within 37.1 ± 1.8 dB for the animation. Even with extremely low ranks ($r < 5$), our method exhibits minimal error drifting over time. Please refer to the supplementary materials for the video reconstructions.

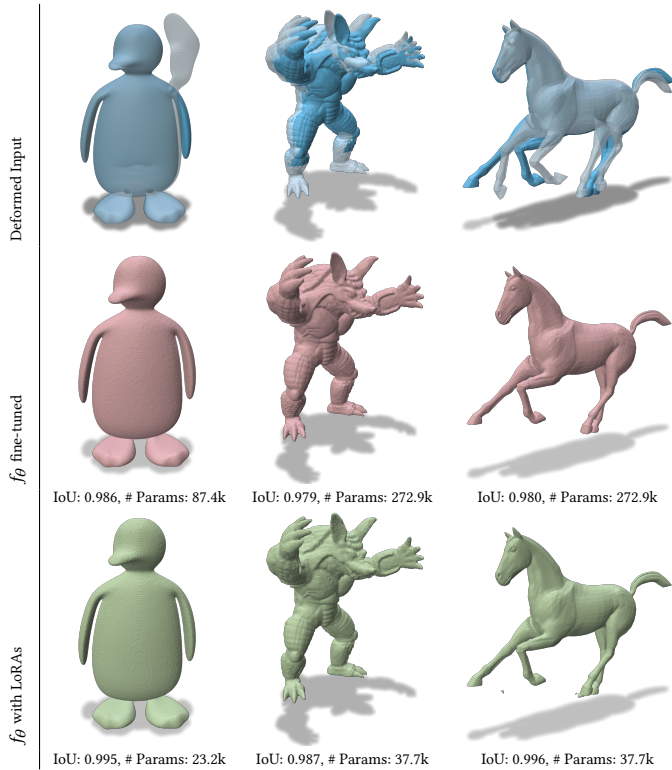


Fig. 4. We encode non-rigid deformations of input surfaces (top row; initial surfaces are translucent) using full fine-tuning of the corresponding base model (middle row) and our LoRA-augmented base model (bottom row). Our method achieves comparable reconstruction quality (measured using IoU) as full fine-tuning while using far fewer additional parameters.

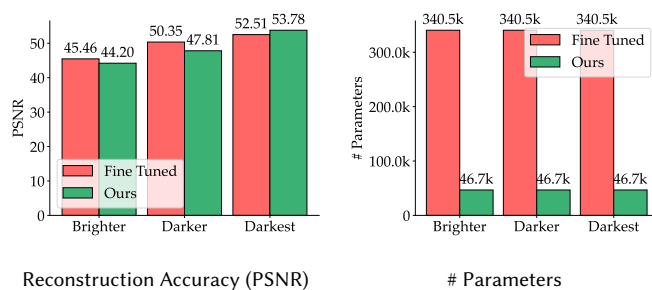


Fig. 5. Comparison of reconstruction quality (PSNR) and parameter count between our approach and full fine-tuning of a base model. Our method reduces the parameter count by over $7\times$ with minimal, barely noticeable reconstruction error (see Figure 2).

7 CONCLUSION

Our results indicate that compact LoRAs are sufficient for encoding small adjustments to instance-specific neural fields with performance competitive to full fine-tuning using an order of magnitude fewer parameters. We demonstrate the versatility of LoRA updates to generic neural field updates with applications in surface deformation, image editing, and video compression. Unlike previous neural

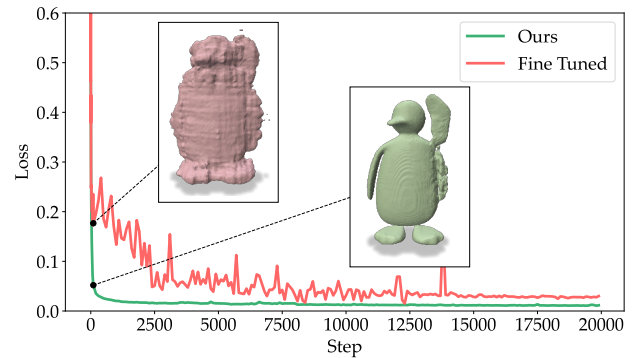


Fig. 6. SDF reconstruction loss (MAPE) during training for our method vs. fine tuning. After only 100 iterations, our LoRA is able to partially encode the surface edit (downward movement of the penguin’s left flipper) while preserving unmodified regions, whereas full fine-tuning introduces significant global distortion.

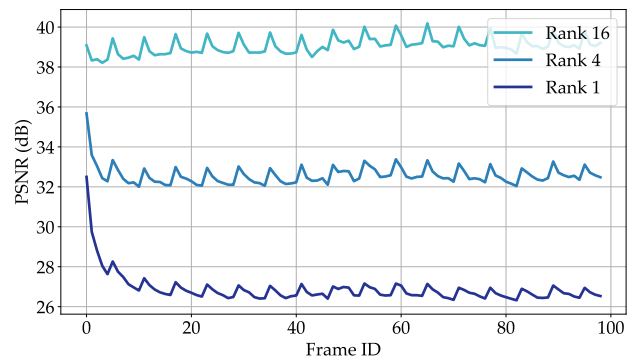


Fig. 7. Per-frame reconstruction accuracy (PSNR) for the highway traffic video (Figure 3) encoded using sequential LoRAs (see §5.3) with varying LoRA ranks.

field fine-tuning works, our LoRAs provide a way to finely control the tradeoff between the expressivity of weight updates and the corresponding size of these updates while still being able to adapt *all* base network weights.

In addition to parameter efficiency, we also observe desirable characteristics in the optimization of LoRA parameters: our neural field LoRAs are noticeably more rapid and stable to train than fully fine-tuning a base neural field. Furthermore, we show empirically that LoRA updates better preserve details in spatial regions of the field that are minimally edited. Beyond representing edits to static fields, our video encoding experiments highlight the feasibility of composing long sequences of LoRAs to encode dynamic data.

Despite its benefits over standard fine-tuning, both our method and fine-tuning are bounded in training throughput by the size and architecture of the pre-trained neural field: as optimizing a LoRA requires computing gradients of the loss with respect to the LoRA parameters, we must backpropagate through the entire base model on every iteration. We leave it as future work to explore ways to incorporate time-efficient LoRA updates in our context.

Another exciting avenue of research is exploring parameter-efficient modifications to neural fields defined implicitly via minimizing energy functionals rather than direct regression of explicit edits (e.g., with surface smoothness energies for SDFs).

ACKNOWLEDGMENTS

The MIT Geometric Data Processing Group acknowledges the generous support of Army Research Office grants W911NF2010168 and W911NF2110293, of National Science Foundation grant IIS2335492 and OAC-2403239, from the CSAIL Future of Data program, from the MIT-IBM Watson AI Laboratory, from the Wistron Corporation, and from the Toyota-CSAIL Joint Research Center

REFERENCES

- Anpei Chen, Zexiang Xu, Andreas Geiger, Jingyi Yu, and Hao Su. 2022. Tensor4: Tensorial radiance fields. In *European conference on computer vision*. Springer, 333–350.
- Hao Chen, Bo He, Hanyu Wang, Yixuan Ren, Ser Nam Lim, and Abhinav Shrivastava. 2021. NeRV: Neural representations for videos. *Advances in Neural Information Processing Systems* 34 (2021), 21557–21568.
- Pei-Ze Chiang, Meng-Shiun Tsai, Hung-Yu Tseng, Wei-Sheng Lai, and Wei-Chen Chiu. 2022. Stylizing 3d scene via implicit representation and hypernetwork. In *Proceedings of the IEEE/CVF Winter Conference on Applications of Computer Vision*. 1475–1484.
- Keenan Crane, Ulrich Pinkall, and Peter Schröder. 2013. Robust fairing via conformal curvature flow. *ACM Transactions on Graphics (TOG)* 32, 4 (2013), 1–10.
- Rishit Dagli, Atsuhiko Hibi, Rahul G Krishnan, and Pascal N Tyrrell. 2024. Nerf-us: Removing ultrasound imaging artifacts from neural radiance fields in the wild. *arXiv preprint arXiv:2408.10258* (2024).
- Thomas Davies, Derek Nowrouzezahrai, and Alec Jacobson. 2020. Overfit Neural Networks as a Compact Shape Representation. *CoRR* abs/2009.09808 (2020). arXiv:2009.09808 <https://arxiv.org/abs/2009.09808>
- Mathieu Desbrun, Mark Meyer, Peter Schröder, and Alan H. Barr. 1999. Implicit fairing of irregular meshes using diffusion and curvature flow. In *Proceedings of the 26th Annual Conference on Computer Graphics and Interactive Techniques (SIGGRAPH '99)*. ACM Press/Addison-Wesley Publishing Co., USA, 317–324. doi:10.1145/311535.311576
- Zekun Hao, Hadar Averbuch-Elor, Noah Snavely, and Serge Belongie. 2020. Dualsdf: Semantic shape manipulation using a two-level representation. In *Proceedings of the IEEE/CVF Conference on Computer Vision and Pattern Recognition*. 7631–7641.
- Soufiane Hayou, Nikhil Ghosh, and Bin Yu. 2024. The Impact of Initialization on LoRA Finetuning Dynamics. *ArXiv* abs/2406.08447 (2024). <https://api.semanticscholar.org/CorpusID:270391476>
- Edward Hu, Yelong Shen, Phillip Wallis, Zeyuan Allen-Zhu, Yuanzhi Li, Shean Wang, Lu Wang, and Weizhu Chen. 2022. LoRA: Low-Rank Adaptation of Large Language Models. In *International Conference on Learning Representations (ICLR 2022)*. <https://openreview.net/forum?id=nZevKeeFY9>
- Takeo Igarashi, Tomer Moscovich, and John F Hughes. 2005. As-rigid-as-possible shape manipulation. *ACM transactions on Graphics (TOG)* 24, 3 (2005), 1134–1141.
- Michael Kazhdan, Jake Solomon, and Mirela Ben-Chen. 2012. Can mean-curvature flow be modified to be non-singular?. In *Computer Graphics Forum*, Vol. 31. Wiley Online Library, 1745–1754.
- Taehwan Kim and Tülay Adalı. 2003. Approximation by fully complex multilayer perceptrons. *Neural computation* 15, 7 (2003), 1641–1666.
- Diederik P Kingma. 2014. Adam: A method for stochastic optimization. *arXiv preprint arXiv:1412.6980* (2014).
- Chenxi Liu, Towaki Takikawa, and Alec Jacobson. 2024a. A LoRA is Worth a Thousand Pictures. arXiv:2412.12048 [cs.CV] <https://arxiv.org/abs/2412.12048>
- Chenxi Liu, Towaki Takikawa, and Alec Jacobson. 2024b. A LoRA is Worth a Thousand Pictures. *arXiv preprint arXiv:2412.12048* (2024).
- Hsueh-Ti Derek Liu and Alec Jacobson. 2019. Cubic stylization. *arXiv preprint arXiv:1910.02926* (2019).
- Hsueh-Ti Derek Liu and Alec Jacobson. 2021. Normal-Driven Spherical Shape Analogies. In *Computer Graphics Forum*, Vol. 40. Wiley Online Library, 45–55.
- Steven Liu, Xiuming Zhang, Zhoutong Zhang, Richard Zhang, Jun-Yan Zhu, and Bryan Russell. 2021. Editing conditional radiance fields. In *Proceedings of the IEEE/CVF international conference on computer vision*. 5773–5783.
- Ziqi Lu, Heng Yang, Danfei Xu, Boyi Li, Boris Ivanovic, Marco Pavone, and Yue Wang. 2024. LoRA3D: Low-Rank Self-Calibration of 3D Geometric Foundation Models. *arXiv preprint arXiv:2412.07746* (2024).
- Lorenzo Luzi, Daniel LeJeune, Ali Siahkoochi, Sina Alemohammad, Vishwanath Saragadam, Hossein Babaei, Naiming Liu, Zichao Wang, and Richard G. Baraniuk. 2024. TITAN: Bringing The Deep Image Prior to Implicit Representations. arXiv:2211.00219 [eess.IV] <https://arxiv.org/abs/2211.00219>
- Julien NP Martel, David B Lindell, Connor Z Lin, Eric R Chan, Marco Monteiro, and Gordon Wetzstein. 2021. Acorn: Adaptive coordinate networks for neural scene representation. *arXiv preprint arXiv:2105.02788* (2021).
- Alessio Mazzucchelli, Adrian Garcia-Garcia, Elena Garces, Fernando Rivas-Manzanque, Francesc Moreno-Noguer, and Adrian Penate-Sanchez. 2024. IReNe: Instant Recoloring of Neural Radiance Fields. arXiv:2405.19876 [cs.CV] <https://arxiv.org/abs/2405.19876>
- Ishit Mehta, Manmohan Chandraker, and Ravi Ramamoorthi. 2022. A level set theory for neural implicit evolution under explicit flows. In *European Conference on Computer Vision*. Springer, 711–729.
- Lars Mescheder, Michael Oechsle, Michael Niemeyer, Sebastian Nowozin, and Andreas Geiger. 2019. Occupancy networks: Learning 3d reconstruction in function space. In *Proceedings of the IEEE/CVF conference on computer vision and pattern recognition*. 4460–4470.
- Ben Mildenhall, Pratul P. Srinivasan, Matthew Tancik, Jonathan T. Barron, Ravi Ramamoorthi, and Ren Ng. 2021. NeRF: representing scenes as neural radiance fields for view synthesis. *Commun. ACM* 65, 1 (Dec. 2021), 99–106. doi:10.1145/3503250
- Vismay Modi, Nicholas Sharp, Or Perel, Shinjiro Sueda, and David I. W. Levin. 2024. Simplicitis: Mesh-Free, Geometry-Agnostic Elastic Simulation. *ACM Trans. Graph.* 43, 4, Article 117 (July 2024), 11 pages. doi:10.1145/3658184
- Thomas Müller, Alex Evans, Christoph Schied, and Alexander Keller. 2022. Instant neural graphics primitives with a multiresolution hash encoding. *ACM transactions on graphics (TOG)* 41, 4 (2022), 1–15.
- Thomas Müller, Alex Evans, Christoph Schied, and Alexander Keller. 2022. Instant Neural Graphics Primitives with a Multiresolution Hash Encoding. *ACM Trans. Graph.* 41, 4, Article 102 (July 2022), 15 pages. doi:10.1145/3528223.3530127
- Jeong Joon Park, Peter Florence, Julian Straub, Richard Newcombe, and Steven Lovegrove. 2019. DeepSDF: Learning continuous signed distance functions for shape representation. In *Proceedings of the IEEE/CVF conference on computer vision and pattern recognition*. 165–174.
- Zhangyang Qi, Yunhan Yang, Mengchen Zhang, Long Xing, Xiaoyang Wu, Tong Wu, Dahua Lin, Xihui Liu, Jiaqi Wang, and Hengshuang Zhao. 2024. Tailor3d: Customized 3d assets editing and generation with dual-side images. *arXiv preprint arXiv:2407.06191* (2024).
- M. Raissi, P. Perdikaris, and G.E. Karniadakis. 2019. Physics-informed neural networks: A deep learning framework for solving forward and inverse problems involving nonlinear partial differential equations. *J. Comput. Phys.* 378 (2019), 686–707. doi:10.1016/j.jcp.2018.10.045
- Silvia Sellán, Noam Aigerman, and Alec Jacobson. 2020. Developability of heightfields via rank minimization. *ACM Trans. Graph.* 39, 4 (2020), 109.
- Viraj Shah, Nataniel Ruiz, Forrester Cole, Erika Lu, Svetlana Lazebnik, Yuanzhen Li, and Varun Jampani. 2025. ZipLoRA: Any Subject in Any Style by Effectively Merging LoRAs. In *Computer Vision – ECCV 2024*, Aleš Leonardis, Elisa Ricci, Stefan Roth, Olga Russakovsky, Torsten Sattler, and Gül Varol (Eds.). Springer Nature Switzerland, Cham, 422–438. doi:10.1007/978-3-031-73232-4_24
- Vincent Sitzmann, Julien Martel, Alexander Bergman, David Lindell, and Gordon Wetzstein. 2020. Implicit neural representations with periodic activation functions. *Advances in neural information processing systems* 33 (2020), 7462–7473.
- Irmak Sivgin, Sara Fridovich-Keil, Gordon Wetzstein, and Mert Pilanci. 2024. Geometric Algebra Planes: Convex Implicit Neural Volumes. *arXiv preprint arXiv:2411.13525* (2024).
- Olga Sorkine and Marc Alexa. 2007. As-rigid-as-possible surface modeling. In *Symposium on Geometry processing*, Vol. 4. 109–116.
- Oded Stein, Eitan Grinspun, and Keenan Crane. 2018. Developability of triangle meshes. *ACM Transactions on Graphics (TOG)* 37, 4 (2018), 1–14.
- Towaki Takikawa, Joey Litalien, Kangxue Yin, Karsten Kreis, Charles Loop, Derek Nowrouzezahrai, Alec Jacobson, Morgan McGuire, and Sanja Fidler. 2021. Neural geometric level of detail: Real-time rendering with implicit 3d shapes. In *Proceedings of the IEEE/CVF Conference on Computer Vision and Pattern Recognition*. 11358–11367.
- Towaki Takikawa, Shunsuke Saito, James Tompkin, Vincent Sitzmann, Srinath Sridhar, Or Litany, and Alex Yu. 2023. Neural Fields for Visual Computing: SIGGRAPH 2023 Course. In *ACM SIGGRAPH 2023 Courses* (Los Angeles, California) (SIGGRAPH '23). Association for Computing Machinery, New York, NY, USA, Article 10, 227 pages. doi:10.1145/3587423.3595477
- Dmitry Ulyanov, Andrea Vedaldi, and Victor Lempitsky. 2018. Deep image prior. In *Proceedings of the IEEE conference on computer vision and pattern recognition*. 9446–9454.
- Yifan Wang, Lukas Rahmann, and Olga Sorkine-Hornung. 2021. Geometry-Consistent Neural Shape Representation with Implicit Displacement Fields. *CoRR* abs/2106.05187 (2021). arXiv:2106.05187 <https://arxiv.org/abs/2106.05187>
- Zhengyi Wang, Cheng Lu, Yikai Wang, Fan Bao, Chongxuan Li, Hang Su, and Jun Zhu. 2024. Prolificdreamer: High-fidelity and diverse text-to-3d generation with variational score distillation. *Advances in Neural Information Processing Systems* 36 (2024).

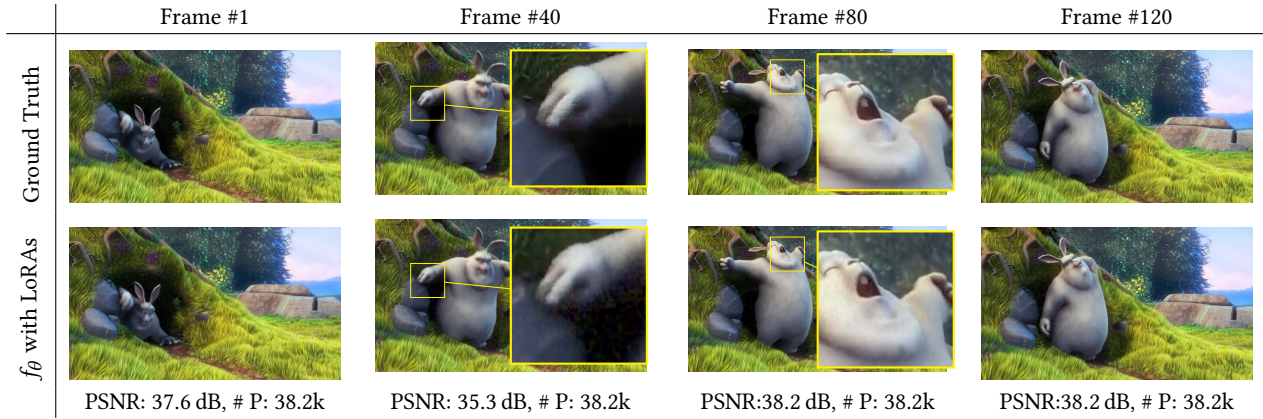


Fig. 8. We also test our sequential LoRA algorithm for encoding an animated sequence. We encode 120 frames from the Big Buck Bunny animation.

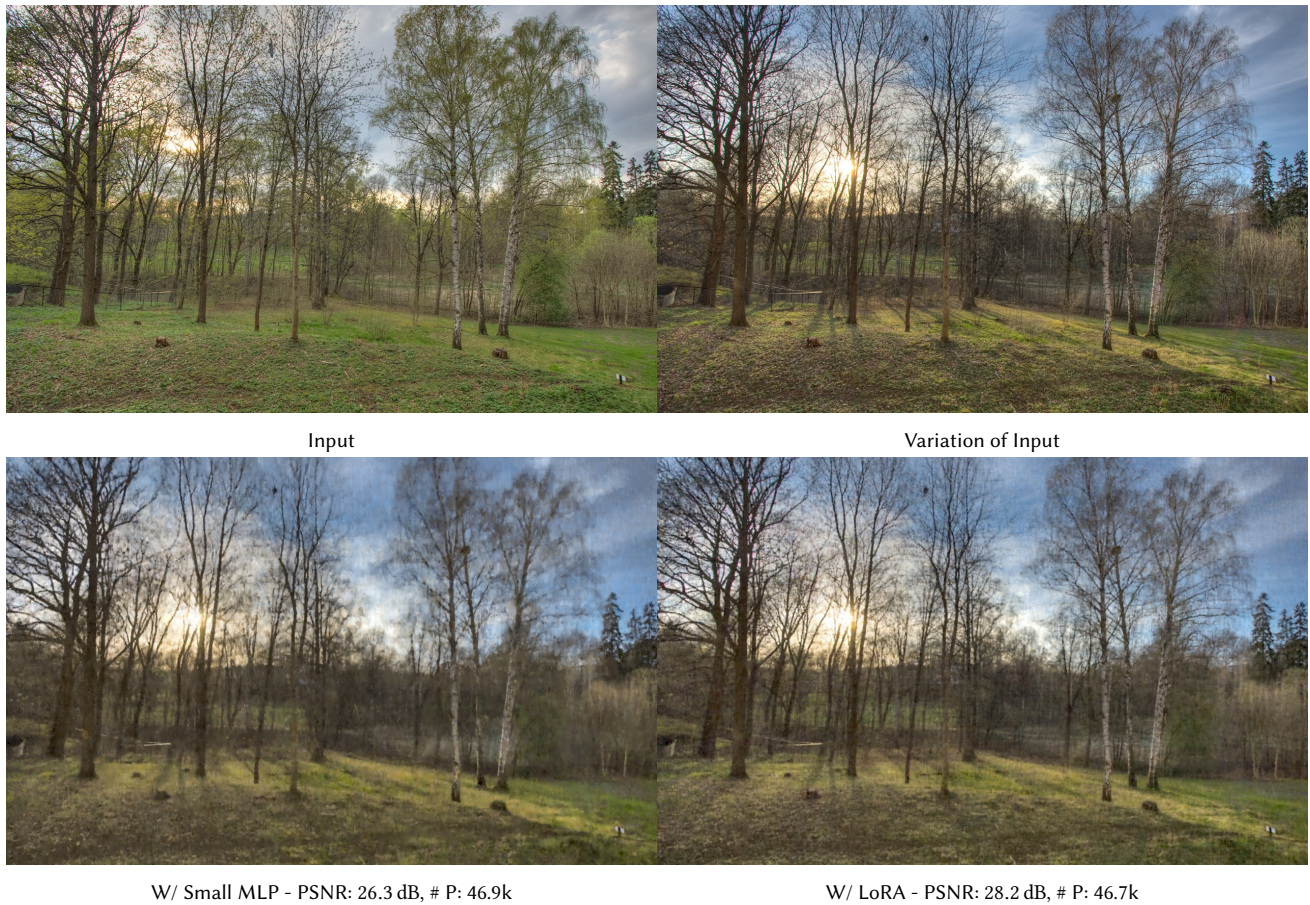


Fig. 9. We compare our LoRA-encoded image variation from the input image with a small MLP containing approximately the same number of parameters as the LoRA. This MLP is trained from scratch to fit the varied image. We see that this baseline MLP (bottom left) is unable to capture as many fine details as our approach (bottom right), suggesting that the LoRA updates preserve relevant information from the pre-trained model it is applied to. Input photos by Eirik Solheim.

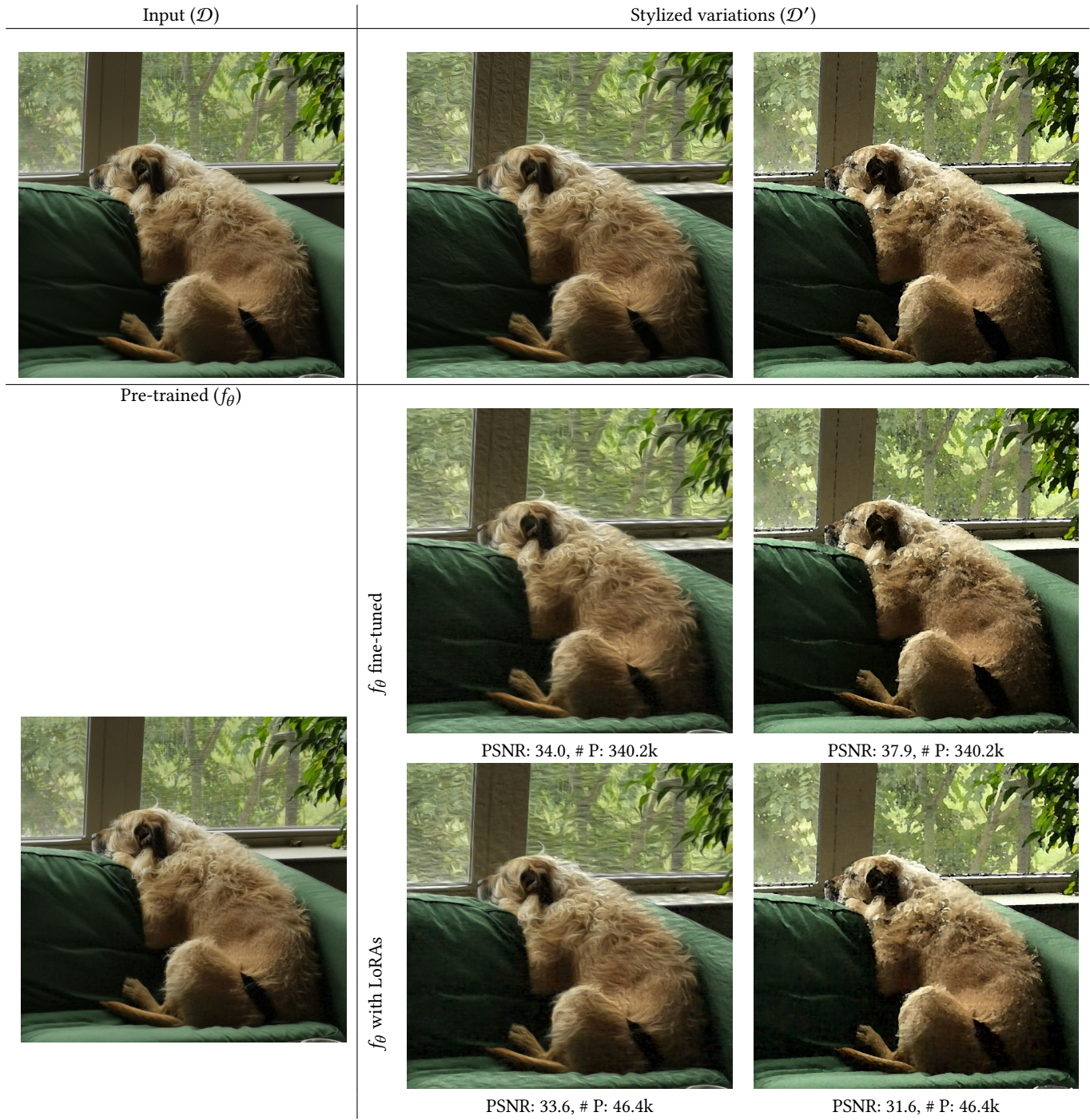


Fig. 10. Similar to Figure 2, we compare full fine-tuning against our LoRA-based method for different variations \mathcal{D}' of a base image \mathcal{D} . Here, the variations arise from digital stylization; an oil painting filter and watercolor filter are applied to \mathcal{D} (top row, middle and right columns) to get \mathcal{D}'